

# Hydrodynamic Model of a Self-Gravitating Optically Thick Gas and Dust Cloud

E. V. Zhukova, A. M. Zankovich, I. G. Kovalenko\*, and K. M. Firsov

*Institute of Physics and Telecommunication, Volgograd State University, Volgograd, 400062 Russia*

Received April 22, 2014; in final form, June 18, 2015

**Abstract**—We propose an original mechanism of sustained turbulence generation in gas and dust clouds, the essence of which is the consistent provision of conditions for the emergence and maintenance of convective instability in the cloud. We considered a quasi-stationary one-dimensional model of a self-gravitating flat cloud with stellar radiation sources in its center. The material of the cloud is considered a two-component two-speed continuous medium, the first component of which, gas, is transparent for stellar radiation and is supposed to rest being in hydrostatic equilibrium, and the second one, dust, is optically dense and is swept out by the pressure of stellar radiation to the periphery of the cloud. The dust is specified as a set of spherical grains of a similar size (we made calculations for dust particles with radii of 0.05, 0.1, and 0.15  $\mu\text{m}$ ). The processes of scattering and absorption of UV radiation by dust particles followed by IR reradiation, with respect to which the medium is considered to be transparent, are taken into account. Dust-driven stellar wind sweeps gas outwards from the center of the cloud, forming a cocoon-like structure in the gas and dust. For the radiation flux corresponding to a concentration of one star with a luminosity of about  $5 \times 10^4 L_{\odot}$  per square parsec on the plane of sources, sizes of the gas cocoon are equal to 0.2–0.4 pc, and for the dust one they vary from tenths of a parsec to six parsecs. Gas and dust in the center of the cavity are heated to temperatures of about 50–60 K in the model with graphite particles and up to 40 K in the model with silicate dust, while the background equilibrium temperature outside the cavity is set equal to 10 K. The characteristic dust expansion velocity is about  $1\text{--}7 \text{ km s}^{-1}$ . Three structural elements define the hierarchy of scales in the dust cocoon. The sizes of the central rarefied cavity, the dense shell surrounding the cavity, and the thin layer inside the shell in which dust is settling provide the proportions  $1 : \{1\text{--}30\} : \{10^{-7}\text{--}10^{-6}\}$ . The density differentials in the dust cocoon (cavity–shell) are much steeper than in the gas one, dust forms multiple flows in the shell so that the dust caustics in the turning points and in the accumulation layer have infinite dust concentration. We give arguments in favor of unstable character of the inverse gas density distribution in the settled dust flow that can power turbulence constantly sustained in the cloud. If this hypothesis is true, the proposed mechanism can explain turbulence in gas and dust clouds on a scale of parsecs and subparsecs.

**DOI:** 10.1134/S1990341315040100

**Keywords:** *interstellar medium: clouds—convection—instabilities—turbulence*

## 1. INTRODUCTION

Star formation in protostellar clouds is governed by a set of physical processes, and the key one among them is turbulence [1, 2]. In order to prevent effectively the gravitational contraction of a cloud, turbulence should have energy exceeding the thermal energy of the cloud material and this means that the turbulence should be near- or supersonic [3–5].

Observations show that gas in interstellar clouds is actually turbulized, with the velocity of turbulent flows being comparable to the sonic one [3, 6].

To maintain both near and supersonic turbulence, permanent powerful energy sources are necessary.

Actually, supersonic turbulence is accompanied by the formation of shock waves, beyond the fronts of which the cloud hot matter is quickly cooled down by de-excitation. The characteristic times of cooling the cloud's gas usually are much shorter than the characteristic dynamical time of the process, the time of free contraction of the cloud [1], therefore turbulent motions should quickly attenuate without consistent energy supply.

In the vast majority of papers, different mechanisms are viewed as possible sources of turbulence: both inner for the physical systems studied (various hydrodynamic or magnetic rotation instabilities, self-gravitation and accretion of contracting gas filaments) and those of external influence (ionization

\*E-mail: [ilya.g.kovalenko@gmail.com](mailto:ilya.g.kovalenko@gmail.com)

fronts, shock waves from supernova outbursts, jet outflows, acceleration of the matter by stellar winds, etc.) [1, 7].

The turbulence maintenance mechanisms of thermal origin, in which inhomogeneous heating of a stratified medium serves as a cause of turbulence, are studied to a far lesser extent. In the case of a permanent source of heating from below and a possibility to cool down because of volume radiation, convective motions should emerge in the medium.

For the purpose of the turbulence thermal mechanism, a number of conditions should be fulfilled simultaneously: (1) there should be sources of heating radiation; (2) heating should be inhomogeneous, consequently, the material of the cloud should be an optically dense medium; (3) the energy of heating radiation transmitted by stars should be partially transformed into excited turbulent motions and partially removed from the system; (4) the gas in the cloud should be stratified.

Point (1) is realized if there are bright young stars in the cloud. The intermediary between cloud's gas and radiation can be interstellar dust. Heating UV radiation of young O and B stars is most effectively absorbed or scattered not by atoms or molecules of gas but by dust particles [8]. At the same time, the cooling of the cloud is most effective in the IR range, for which the cloud material is almost transparent. Thus, points (2) and (3) can be fulfilled in the case of gas and dust clouds. The cloud material can be stratified, e.g., due to its own gravity; consequently, the effect, if any, should manifest itself on Jeans scales. Therefore, the conditions of point (4) are fulfilled for massive self-gravitating clouds.

It is necessary to have an optical-dynamical reference model of a self-gravitating optically dense gas and dust medium to develop a theory on thermal turbulence in interstellar clouds.

As a first step, it is natural to consider a model in which the material distribution in the cloud is assumed to be in a steady state. In [9] a cloud hydrostatic model is designed in which dust is considered "frozen-in" into surrounding gas; the cloud itself is viewed as a gas and dust flat layer of indefinite extent.

In the present paper, we develop a hydrostatic model in order to take into account possible relative motions of gas and dust. The state of the medium is no more assumed to be static, although, the flow is considered steady-state, i.e., the model turns from hydrostatic into hydrodynamic, but describing the steady flow. We hold on to the planar geometry of the cloud, accepted in [9]. The choice of this geometry is largely determined by relative simplicity of radiation transfer calculation and, naturally, limits the class of the objects studied to extended flat clouds. As is

shown below, the unstable nature of the material distribution in the cloud, predicted within the framework of the planar model, should also occur in the cases of other geometries of the cloud. In next papers, we will continue to develop the model in order to consider the finitude of cloud dimensions.

Notice that flows of dust-driven wind have been studied by different authors to analyze the structure of circumstellar dust shells and atmospheres of giants, C stars, and long-period variables [10–15], T Tauri stars [16] or brown dwarfs [17, 18]. All those problems concerned small scales in which self-gravity was inconsiderable. Larger linear scales (1–10 pc) and, consequently, masses (of the order of  $10^4 M_{\odot}$ ) correspond to gas and dust winds in emission nebulae. Although Ochsendorf et al. [19, 20] noted the importance of self-gravity, they did not take it into consideration in their models. Different scenarios of keeping the interstellar gas in balance, of gas acceleration or turbulization through radiation pressure on the dust frozen in gas on even larger scales (of the order of stellar cluster scales) have been investigated in many papers [21–23], but as a rule, the analysis is semiquantitative without calculating a detailed structure of the flow. Gas dynamical instabilities occurring through the force impact of radiation on a gas and dust medium have been known since Field's paper [24]. Numerical modelling confirms the turbulence emergence due to the instability development [17, 18, 25]. However, the influence of radiation pressure, gas and dust relative motion, and self-gravitation have not been simultaneously considered in any paper in which different scenarios of turbulence generation in interstellar clouds are discussed. A problem similar to that considered in the present paper has not been set so far.

Section 2 introduces the formulation of the problem and the construction of the cloud physical model. We discuss in detail the processes of interaction of gas with dust and with radiation, establish basic equations of radiation hydrodynamics: the equations of hydrostatic equilibrium for gas, the equations of motion for dust, and also the equations of radiation transfer and radiative equilibrium. In Section 3 we give basic equations of the model in the dimensionless form, which is convenient for numerical integration, list basic parameters of the model, and describe boundary conditions and the procedure of calculation. The results of the numerical calculations for different parameters are presented in Section 4, Section 5 is dedicated to the discussion of the obtained results.

## 2. PHYSICAL MODEL OF A GAS AND DUST CLOUD

### 2.1. General Assumptions and Simplifications in the Model

The H II regions in the vicinity of OB stars filled with warm or hot ionized gas with a temperature of about  $10^7$  K in the center of a rarified cavity can serve as the best example of the objects in which gas and dust flows, accelerated by the stellar radiation pressure, form and, to some extent, as the prototypes for our model of gas and dust stellar wind in clouds. The H II regions also contain cool dense shells of gas and dust with temperatures of 10–100 K, radiating in the IR range. Characteristic bubble sizes of about 1–20 pc in dense clouds with gas concentrations of approximately  $10^2$ – $10^6$  cm $^{-3}$  are reached at luminosities of central stars, the sources of gas and dust wind, of the order of  $L/L_{\odot} \gtrsim 10^5$  [26].

Observations of the H II bubbles in the IR range show a considerable amount of dust in them. Almost all the H II regions known in the Galaxy have maximum IR radiation at a wavelength  $\lambda \approx 100$   $\mu$ m which indicates the presence of dust with a temperature of about 30 K [26].

As a characteristic object, let us consider the emission nebula Sh2-292, which is a gas and dust cloud of a round shape surrounding a massive young bright B0e star HD 53367 with a luminosity of  $1.7 \times 10^5 L_{\odot}$  [27]. The object Sh2-292 is a part of the nebula IC 2177 (Seagull nebula), its transverse dimension is at least 3 pc.

A color image of the nebula<sup>1</sup> obtained at the La Silla observatory and published by ESO in 2012 gives an idea of the nebula structure. Strong ultraviolet radiation from the star ionizes the nebula gas. In the H II regions, the gas emits in lines (bright red colors in the nebula image), and the dust scatters the radiation (consequently, light blue colors). Regions of luminous half-transparent cloud material alternate with extended black dust bands. The nebula photo makes it possible to distinguish details of different scales in the gas and dust which are typical of a turbulized medium.

Let us emphasize that in the present paper we did not aim to construct a model of any specific object. In the first place, we are interested in physical mechanisms of self-supporting turbulence generation. This allows us to simplify the model by avoiding consideration of specific details which are not essential to be taken into account when analyzing general physical mechanisms. For example, we rule out electromagnetic action at a distance between the particles of the medium.

The electric charge of dust particles is important for dynamics. Indeed, under the influence of strong ionizing radiation of the star, a dust particle acquires a charge  $Z$  of tens to thousands units depending on its size and chemical composition [20].

In a magnetic field, the charged dust particle performs Larmor motion along the magnetic field lines. In the case of a strong magnetic field with energy density comparable to the thermal or kinetic energy of stellar wind particles, one should expect indications of anisotropy in the shape of the H II bubble. However, many emission nebulae have near-spherical shapes (the above-mentioned nebula Sh2-292, nebulae RCW 82 and RCW 120 [19]), which means that either magnetic field lines are directed radially and the magnetic field does not influence the radial scattering of the particles or the intensity of the magnetic field is low. This allows us to rule out the Lorentz force magnetic component in our model.

The electric component of the Lorentz force manifesting itself through Coulomb friction can turn out to be more significant for the charged particle motion in an ionized medium. The calculations from [20] with the formulae following from the kinetic theory of ionized gases (see, e.g., [28]) show that for particles with a charge  $Z \approx 200$  and 2000 in a medium with a characteristic temperature  $T \sim 50$  K and a concentration  $n_{\text{H}} \sim 10$  cm $^{-3}$  at a distance of 0.1 pc from a star with a luminosity of about  $10^5 L_{\odot}$ , Coulomb friction for a silicate particle about  $10^3$  times exceeds the collisional one. In such conditions, the relaxation length (a characteristic distance at which the charged dust particle loses its initial speed and comes to equilibrium with the medium) amounts to thousandths of a parsec. It means that the dust particles should be considered frozen-in into the matter, and the gas and dust matter should not be separated into two components. We have already studied such a one-fluid model of gas and dust wind in [9]. Here we would like to investigate possible effects associated with the separation of gas and dust motions.

The paper [20] is worth noting, where the authors cast doubt on theoretical estimates of the Coulomb friction value. The authors noted a high degree of uncertainty (with an accuracy up to one order) of the experimental results in estimating the photoionization efficiency, and the effect of spontaneous electric polarization of thin films (materials which model cosmic dust particles in laboratory experiments), which considerably improves the work function [29]. Finally, the authors' comparison of their numerical modeling results with and without consideration of the Coulomb constituent of the friction force showed a discrepancy between observations and calculations with Coulomb friction and, vice versa, agreement between observations and the model without Coulomb

<sup>1</sup><http://www.eso.org/public/news/eso1237/>

friction. Consistent with the paper [20], we take into account the Coulomb constituent of the friction force as a value which does not considerably differ from the collisional constituent: we assign the ratio of the Coulomb force to the collisional force in the interval of 0–3. Simplifications that we used—the neglect of effects associated with strong ionization of gas (immediate radiation pressure on gas, weak Coulomb friction)—actually indicate that the present model is constructed for HI clouds.

### 2.2. Geometry and Physicochemical Composition of the Cloud in the Model

We view the cloud as a gas and dust layer of indefinite extent being in the state of dynamic equilibrium and inhomogeneous along the  $z$  coordinate, which we agree to call vertical. We consider the cloud to be reflection symmetric with respect to the equatorial plane  $z = 0$ , and this allows us to restrict the solution for only one half of the cloud over its width.

We consider the gas and dust medium in the cloud as a double-component and double-velocity fluid which is characterized by mass densities of gas  $\rho_g$  and dust  $\rho_d$ , and by the velocities  $\mathbf{v}_g$  and  $\mathbf{v}_d$  respectively. In doing so, we consider the gas more massive ( $\rho_g \gg \rho_d$ ) and motionless ( $\mathbf{v}_g = 0$ ).

We consider the gas constituent of the cloud as an ideal gas with the adiabatic index  $\gamma = 5/3$ . We assume the gas to be in the atomic hydrogen form, the distribution by species (molecular hydrogen, helium, etc.) is not taken into account.

The mass of the cloud is regarded large if compared to the mass of radiating stars, we thus take into consideration only the proper gravitational field of the cloud.

We suppose that radiation sources are situated at the center of the cloud in the plane  $z = 0$  and are uniformly distributed along the plane and emit isotropically.

It is supposed that the dust under the radiation pressure of the sources is swept out from the center of the cloud to the periphery. It is implied, however, that the dust is either generated in the center of the cloud by old giant stars or swept out from the dust shell preserved during the star formation process. We suppose that such a dust outflow outward from the center of the cloud is stationary. At the same time, the gas is considered transparent relative to the radiation from the sources, and the radiation influence immediately on the gas particles is inconsiderable. The radiation influence on the gas is indirect and due to the friction of the swept-out dust and the gas. In directions perpendicular to the  $z$  axis, we suppose equilibrium, i.e., the balance of the pressure and self-gravitation forces. Gradients along the mentioned directions are

considered small if compared to the corresponding gradient along  $z$ , which allows us to disregard them and consider the gas to be homogeneous along directions perpendicular to  $z$ . This, in fact, corresponds to the Jeans approximation. By this means, we finally assume the gas to be quiescent.

Notice that the medium is collisional enough to provide equalizing of the gas and dust temperature at times which are small if compared to the time of passing the halfwidth of the cloud by a dust grain  $t_{\text{dyn}} \sim 10^6$  Myr (the detailed estimation of the so-called dynamical time of the problem  $t_{\text{dyn}}$  is given in Section 4.2). If one takes  $T_d = 30$  K as the characteristic temperature of a dust grain in our model, the gas temperature  $T_g = 100$  K and gas concentration  $n_g = 10^2\text{--}10^6$  cm $^{-3}$ , then the characteristic time of the equalizing of gas and dust temperatures for a graphite grain with a radius of 0.1  $\mu\text{m}$  amounts to [30]

$$t_{\text{rel}} \approx \frac{E}{\frac{dE}{dt}} \approx \frac{4\pi a^3 \rho_{\text{grain}} C T_d}{3n_g \sqrt{\frac{8k_B T_g}{\pi m_g}} \pi a^2 2k_B (T_g - T_d)} \quad (1)$$

$$\approx (3 \times 10^{-8} \text{--} 3 \times 10^{-4}) t_{\text{dyn}}$$

$$= (3 \times 10^{-2} \text{--} 3 \times 10^2) \text{ yr.}$$

Here  $E$  is the thermal energy of the dust grain,  $C$  is the specific heat capacity of graphite, which equals  $1.39 \times 10^4$  erg/(g $\times$ K) for  $T \sim 100$  K,  $\rho_{\text{grain}}$  is the density of the dust grain, which usually varies in the range of 1.8–3.5 g/cm $^3$  [31].

A notable imbalance in gas and dust temperatures can be seen either at short distances near dust sources (however, with regard to estimate (1), the characteristic length will be equal to one calculation grid cell) or far on the periphery of the gaseous cloud, where gas concentration is small.

In this connection, we consider the temperature of both components similar and equal to  $T$ .

### 2.3. Interaction between Radiation and the Matter of the Cloud

The optical part of the model is a solution of the problem on radiative transfer of energy. As an optically dense medium, we have a set of dust particles of a certain size and chemical composition being illuminated by a beam of light with preset intensity and frequency.

The interaction between radiation and dust will be viewed in the two-channel approximation. We suppose that the maximum of stellar radiation falls within the ultraviolet range, the dust component for which has a considerable optical depth; therefore, the UV

radiation transfer is calculated with regard to its interaction with dust. Then the energy gained in this process is partially converted into translational motion energy, which is taken into consideration in the model with the pressure of the radiation on the dust, and is partially radiated in the IR range, relative to which the medium is considered to be transparent.

It is natural to set the boundary conditions in terms of optical depth  $\tau$ , which we will measure from the center of the cloud  $z = 0$ , in the following way. As the radiation source is situated in the center of the cloud, then apart from the direct radiation from the source  $F_0$ , which fall onto the inner boundary of the cloud ( $\tau = 0$ ), the reflected diffuse radiation from the other part of the cloud will affect the matter:

$$F_0^\downarrow(\tau = 0) = F_0^\uparrow(\tau = 0). \quad (2)$$

Here with the up and down arrows, we denote the upward (in the negative  $z$  direction) and the downward (in the positive  $z$  direction) flows of the diffuse radiation respectively.<sup>2</sup>

The outer boundary ( $\tau = \tau_h$ ) of the cloud is considered absolutely black, i.e., the radiation freely escapes the boundary, which corresponds to the absence of diffuse radiation sources from outside:

$$F_0^\uparrow(\tau = \tau_h) = 0. \quad (3)$$

Intensity of scattering radiation will depend only on the  $z$  coordinate and the direction of radiation propagation, characterized by a zenith angle  $\theta$ , i.e., the angle between the direction of radiation propagation and the  $z$  axis.

Thus, in order to determine the variation of intensity of the radiation passing through the absorbing, scattering, and radiating medium consisting of plane-parallel layers, it is necessary to solve the equation

$$\mu \frac{dI_\nu}{d\tau} = -I_\nu + \frac{\omega}{2} \int_{-1}^1 I_\nu(\mu, \mu'; \tau) p(\mu, \mu') d\mu' + \varepsilon_\nu, \quad (4)$$

where  $I_\nu = I_\nu(\tau)$  is the target intensity of radiation at a frequency  $\nu$ ;  $p(\mu, \mu')$  is the scattering indicatrix characterizing the scattering of the radiation which comes from the direction  $\mu' = \cos\vartheta'$  in the direction  $\mu = \cos\vartheta$ ;

$$\omega = \frac{\sigma_\nu}{\sigma_\nu + k_\nu} \quad (5)$$

is an albedo of a single scattering, determining the possibility that a photon will be scattered but not

absorbed;  $\sigma_\nu$  and  $k_\nu$  are the coefficients of scattering and absorption respectively, which add up to the attenuation coefficient  $\alpha_\nu = \sigma_\nu + k_\nu$ ;

$$\varepsilon_\nu(\tau) = \frac{1}{2} F_0 \delta(\mu - \mu_0) e^{-\tau/\mu_0} \quad (6)$$

is the radiation coefficient with regard to the radiation from the star as the only UV radiation source in the model;  $\mu_0$  is the cosine of the angle between the normal to the surface and the direction of incidence of the photons from the source.

We will determine the certain values of the coefficients of attenuation, scattering, and absorption by Mie theory [32].

To be specific, let us assume that the dust is represented in graphite particles of a similar size  $a_0$  and mass  $m_d$ , as this is the most widely spread material of dust particles in the interstellar medium [33]. For comparison, we present the results of a single calculation of the gas and dust cloud structure for the case of silicate particles.

To determine the coefficients of attenuation, absorption, and scattering, it is necessary to know the size distribution function of dust particles. The size distribution function of dust particles for a monodisperse compound appears as follows:

$$\int_{a_{\max}}^{a_{\min}} n(a) da = \int_{a_{\max}}^{a_{\min}} n_d \delta(a - a_0) da, \quad (7)$$

here  $n_d$  is a complete concentration of dust particles.

In order to accurately determine the contribution of the diffuse constituent of radiation into the interaction of the radiation and the medium, it is necessary to preset the scattering indicatrix. We are considering particles with sizes of 0.2  $\mu\text{m}$  at most, comparable to the UV radiation wavelength. In this case, the Henyey–Greenstein phase function [34] can be chosen as an approximation for the scattering indicatrix:

$$p \cos \vartheta = \frac{1 - g_{\text{HG}}^2}{(1 + g_{\text{HG}}^2 - 2g_{\text{HG}} \cos \vartheta)^{3/2}}, \quad (8)$$

where the parameter  $0 \leq |g_{\text{HG}}| \leq 1$  characterizes the degree of slenderness of the indicatrix forward: the closer it is to unity, the greater the slenderness is.

Proper infrared radiation of the dust particles cools them down carrying thermal energy away by reradiated photons. It is possible to determine the temperature of the “dust–gas” mixture from the balance of energy income and outflow.

The rate of heating of a dust grain [8]

$$\frac{dE^+}{dt} = \int_0^\infty k_\nu J_\nu d\nu, \quad (9)$$

<sup>2</sup>When determining the direction of the flows, we follow the tradition accepted in atmospheric optics, where the flow from the source is considered downward.

here  $J_\nu$  is the average intensity of radiation at a preset frequency  $\nu$ , which is averaged over all directions. The absorption efficiency varies comparatively little with frequency, and the equation can be written in the following way:

$$\frac{dE^+}{dt} \approx kJ, \quad (10)$$

where  $k$  is the coefficient of absorption of stellar radiation by dust at some effective frequency which, in our case, corresponds to the frequency of UV radiation. The dust particle is cooled down by radiation from its entire surface. For spherical particles, the cooling rate equals [8]

$$\frac{dE^-}{dt} = \int_0^\infty k_\nu B_\nu(T) d\nu \approx k_* \frac{\sigma_{\text{SB}}}{\pi} T^4, \quad (11)$$

where  $B_\nu(T)$  is the Planck function,  $\sigma_{\text{SB}}$  is the Stefan–Boltzmann constant,  $k_*$  is the coefficient of proper radiation of the particle.

Eventually, the total energy absorbed by the matter in thermal equilibrium is equal to the total energy radiated by it, i.e., the radiative equilibrium condition is fulfilled [35]:

$$\int_0^\infty k_\nu J_\nu d\nu = \int_0^\infty k_\nu B_\nu(T) d\nu. \quad (12)$$

In our review, where we simultaneously consider two effects—the heating by the UV radiation and the cooling by the radiation in the IR range of the spectrum—the equation of radiative energy balance can be written in the following way:

$$kJ = k_* \frac{\sigma_{\text{SB}}}{\pi} T^4. \quad (13)$$

Notice that apart from stellar radiation, there are other heating sources in the interstellar medium, for example, cosmic rays. At low temperatures of the order of 10 K, the dissipation in turbulent gas can serve as the dominating heating source [36]. The radiation in lines serves as the gas cooling source owing to collisions of its atoms and photons. Thus, additional sources and sinks of energy should be taken into consideration in balance equation (13). We know that if there is no energy source in the center of a dense cloud, its typical temperatures  $T_b \approx 10\text{--}20$  K [8, 37]. It is the case when thermal radiation from the cloud would be determined with this typical temperature. In this case, the balance equation can be written as follows:

$$kJ + W_b = k_* \frac{\sigma_{\text{SB}}}{\pi} T^4, \quad (14)$$

where the summand  $W_b = k_* \frac{\sigma_{\text{SB}}}{\pi} T_b^4$  is the loss by proper radiation of dust at the equilibrium background temperature  $T_b$  in thermal balance conditions with the absence of a stellar radiation source.

In the present model, the dust is an intermediary between the radiation and gas. In the extreme case, when there is no dust at all, gas becomes absolutely transparent for radiation and we consider it as adiabatic.

#### 2.4. Interaction of the Gas and Dust Components of the Cloud

Resistance force from the surrounding medium influences a moving dust grain. The friction force consists of the collisional and Coulomb constituents [28].

In the case when the dust grain velocity is considerably lower than the thermal velocity of gas atoms, the friction force is directly proportional to the mass velocity of dust particles, in the reverse extreme case it is quadratic in velocity. Finally, the friction force can be written in the following way [38]:

$$\mathbf{F}_d = (1 + \xi)n_g a^2 \Delta \mathbf{v} \sqrt{\frac{128\pi}{9} k_B T m_g + \pi^2 m_g^2 (\Delta \mathbf{v})^2}, \quad (15)$$

here  $n_g$  is the gas concentration,  $k_B$  is the Boltzmann constant,  $\xi$  is the ratio between the Coulomb and collisional constituents of the friction force,  $\Delta \mathbf{v} = \mathbf{v}_g - \mathbf{v}_d = -\mathbf{v}_d$  is the relative velocity of component motions.

It is convenient to introduce a fiction coefficient  $\beta$ , which is determined by the relation

$$\frac{\mathbf{F}_d}{m_d} = \beta \Delta \mathbf{v}. \quad (16)$$

The equation of the dust grain motion which is affected by the friction force caused by gas is written in the form

$$\frac{d\mathbf{v}_d}{dt} = \beta \Delta \mathbf{v}. \quad (17)$$

On the other hand, in view of (16), equation (17) can be written as

$$\rho_d \frac{d\mathbf{v}_d}{dt} = \mathbf{F}_d n_d.$$

In this case, the equation of motion of a unit volume gas particle is

$$\rho_g \frac{d\mathbf{v}_g}{dt} = -\mathbf{F}_d n_d.$$

Hence, the acceleration for gas can be written as follows:

$$\frac{d\mathbf{v}_g}{dt} = -\beta \Delta \mathbf{v} \frac{\rho_d}{\rho_g}. \quad (18)$$

### 2.5. Radiation Hydrodynamics

The matter in the cloud on the scale of the problem can be considered as a continuous medium.

If the gas in the cloud is in hydrostatic equilibrium, the weight of the overlying gas layers is resisted by the dust friction force and gas pressure.

The gas pressure is estimated from the ideal gas law

$$P_g = \frac{\rho_g k_B T}{m_g}, \quad (19)$$

where  $m_g$  is the average mass of a gas particle.

The equation which determines the condition of force balance for the gaseous component along the

vertical coordinate, taking the gravitational and friction forces into account (18), can be written in the form:

$$-\frac{1}{\rho_g} \frac{dP_g(z)}{dz} - \frac{d\Phi(z)}{dz} + \frac{\beta v_d(z) \rho_d(z)}{\rho_g(z)} = 0. \quad (20)$$

The dust is viewed as a component that does not have proper pressure. Equilibrium vertical motion of dust is determined by the gravitational force, friction, and radiation pressure. The equation of dust motion regarding (17) appears as follows:

$$v_d(z) \frac{dv_d(z)}{dz} = -\frac{d\Phi(z)}{dz} + \frac{4\pi}{c \rho_d(z)} \int_0^\infty (k(z, \nu) + (1 - g_{HG}) \sigma(z, \nu)) H(z, \nu) d\nu - \beta v_d(z). \quad (21)$$

Above,  $k(z, \nu) \equiv k_\nu$ ,  $\sigma(z, \nu) \equiv \sigma_\nu$ , and  $H(z, \nu)$  is the entire flux of radiation.

Here the friction coefficient  $\beta$  in accordance with (15) and (16) is determined as

$$\beta = \frac{(1 + \xi) \pi a^2 m_g n_g(z)}{m_d} \left( \left( \frac{8\sqrt{2} c_s(z)}{3\sqrt{\pi\gamma}} \right)^2 + v_d^2(z) \right)^{\frac{1}{2}}, \quad (22)$$

where the speed of sound in polytropic gas is  $c_s(z) = \sqrt{\gamma P_g(z) / \rho_g(z)}$ .

Gravitational potential  $\Phi(z)$  can be found from Poisson's equation

$$\frac{d^2 \Phi(z)}{dz^2} = 4\pi G (\rho_g(z) + \rho_d(z)). \quad (23)$$

For dust, one should add the continuity equation, which in a stationary case reduces to the law of conservation of dust mass flux

$$\rho_d(z) v_d(z) = Q_d = \text{const.} \quad (24)$$

We close the system with the equation of radiative transfer (4), which determines the variation of radiation intensity when passing through an absorbing, scattering, and radiating medium. Knowing the radiation intensity in the medium  $I_\nu(z)$ , we can calculate the average intensity  $J_\nu(z)$  and the radiation flux  $H_\nu(z)$  as the zero and first momenta of intensity over  $\nu$  respectively.

## 3. MATHEMATICAL MODEL

### 3.1. Basic Equations and Control Parameters of the Model

Let us make the physical variables of the problem dimensionless in the following way:

$$\begin{aligned} \tilde{\rho}_g &= \frac{\rho_g}{\rho_{g0}}, & \tilde{\rho}_d &= \frac{\rho_d}{\rho_{g0}}, & \tilde{v}_d &= \frac{v_d}{c_{s0}}, \\ \tilde{P}_g &= \frac{P_g}{\rho_{g0} c_{s0}^2}, & \tilde{\Phi} &= \frac{\Phi}{c_{s0}^2}, & \tilde{z} &= \frac{z}{\lambda_J}, \\ \tilde{T} &= \frac{T}{T_0}, & \tilde{c}_s &= \frac{c_s}{c_{s0}}, & \tilde{\alpha} &= \frac{\alpha}{\alpha_0}, \\ \tilde{k} &= \frac{k}{\alpha_0}, & \tilde{k}_* &= \frac{k_*}{\alpha_0}, & \tilde{\sigma} &= \frac{\sigma}{\alpha_0}, \\ & & \tilde{H} &= \frac{H}{H_0}. \end{aligned} \quad (25)$$

Further, we drop the index  $\nu$  for all the optical values, as we take into account the transfer at one frequency only. In system (25), all the values marked with the index "0" are taken as the corresponding characteristic physical variables; the precise determination of these values through dimensionless control parameters of the problem is given below. Along with this, the characteristic temperature and mass density of gas are associated with the characteristic speed of sound

and gas concentration:

$$T_0 = \frac{c_{s0}^2 m_g}{\gamma k_B}, \quad \rho_{g0} = m_g n_{g0}. \quad (26)$$

We introduce the characteristic flux  $H_0$  as the flux of thermal energy radiated from some surface with the temperature  $T_0$ :

$$H_0 = \sigma_{SB} T_0^4. \quad (27)$$

The value

$$\alpha_0 = \frac{3\pi\rho_{g0}}{2\lambda\rho_{\text{grain}}} \quad (28)$$

has the meaning of the inverse mean free path of a photon. Here  $\lambda = c/\nu$  is a wavelength of the source radiation. The Jeans scale is determined by the relation

$$\lambda_J = \frac{c_{s0}}{\sqrt{4\pi G\rho_{g0}}}. \quad (29)$$

With regard of the introduced designations, the system of equations for dimensionless variables reduces to the form

$$\begin{aligned} 0 &= -\frac{1}{\tilde{\rho}_g} \frac{d\tilde{P}_g}{d\tilde{z}} - \frac{d\tilde{\Phi}}{d\tilde{z}} + \tilde{\beta} \frac{\tilde{\rho}_d}{\tilde{\rho}_g} \tilde{v}_d, \\ \tilde{v}_d \frac{d\tilde{v}_d}{d\tilde{z}} &= -\frac{d\tilde{\Phi}}{d\tilde{z}} + \tau_0 R \frac{(\tilde{k} + (1 - g_{HG})\tilde{\sigma}) \tilde{H}}{\tilde{\rho}_d} - \tilde{\beta} \tilde{v}_d, \\ \frac{d^2\tilde{\Phi}}{d\tilde{z}^2} &= \tilde{\rho}_g + \tilde{\rho}_d, \quad \tilde{\rho}_d \tilde{v}_d = \tilde{Q}_d, \quad \tilde{P}_g = \frac{\tilde{\rho}_g \tilde{T}}{\gamma}, \end{aligned} \quad (30)$$

$$\frac{d\tilde{H}}{\tau_0 d\tilde{\tau}} = \tilde{J} - \tilde{S}, \quad \pi\tilde{k}\tilde{J} + \tilde{k}_* \tilde{T}_b^4 = \tilde{k}_* \tilde{T}^4,$$

$$\tilde{S} = \frac{\omega}{2} \int_{-1}^1 \tilde{I}(\mu, \mu'; \tilde{\tau}) p(\mu, \mu') d\mu' d\mu + \frac{\tilde{F}_0}{2} e^{-\frac{\tilde{\tau}}{\mu_0}},$$

$$\tilde{\tau} = \int_0^{\tilde{z}} \tilde{\alpha} d\tilde{z}, \quad \omega = \frac{\tilde{\sigma}}{\tilde{\sigma} + \tilde{k}},$$

$$\tilde{\sigma} = \tilde{\rho}_d Q_s(x, m)/x, \quad \tilde{\alpha} = \tilde{\rho}_d Q_{\text{ext}}(x, m)/x,$$

$$\tilde{k} = \tilde{\rho}_d Q_a(x, m)/x, \quad \tilde{k}_* = \tilde{\rho}_d Q_a(x_*, m)/x_*. \quad (31)$$

Here  $\tilde{S}$  is the dimensionless source function. The efficiency factors of attenuation  $Q_{\text{ext}}$ , absorption  $Q_a$ , and scattering  $Q_s$  of the radiation by the medium can be calculated with the standard formulae [39]. We

characterize the dimensionless radius of a dust grain with the diffraction parameter [39]

$$x = \frac{2\pi a}{\lambda}. \quad (32)$$

The value  $x_*$  is determined similarly to (32), where  $\lambda$  is substituted by the wavelength of the proper radiation of a dust grain  $\lambda_*$ . The size of the dust grain  $a$  is chosen in the range of 0.05–0.15  $\mu\text{m}$ . Correspondingly, for the ultraviolet radiation with a wavelength of 0.22  $\mu\text{m}$ , we have  $x = 1.4$ –4.3. For the proper radiation of the dust grain, the wavelength of which we set in the long-wave infrared range  $\lambda_* = 100 \mu\text{m}$  that corresponds to dust grain temperatures of 10–40 K, we have  $x_* = 0.002x$ . For the size range under consideration, we assume the asymmetry parameter  $g_{HG}$  to be 0.23–0.68.

The complex refractive index of the dust grain  $m$  for different wavelengths is chosen to be  $m = 2.1 + i \times 1.5$  [40] and  $m_* = 10.39 + i \times 9.592$  [41] for the graphite particle, and  $m = 1.707 + i \times 0.166$ ,  $m_* = 2.723 + i \times 0.240$  [42] for the silicate particle.

Apart from the two microscopic spatial scales  $a$  and  $\lambda$  (and  $\lambda_*$  too), there are two macroscopic spatial scales in the problem: gravitational  $\lambda_J$  and optical  $l_{\text{ph}} = \alpha_0^{-1}$  (mean free path of a photon). The ratio of these scales determines the dimensionless control parameter of the problem

$$\tau_0 = \frac{\lambda_J}{l_{\text{ph}}} = \alpha_0 \lambda_J, \quad (33)$$

which has the meaning of characteristic optical depth of the cloud. For graphite particles with the indicated sizes, the gas concentration considered in our model  $n_{g0} \sim 10^2$ – $10^6 \text{ sm}^{-3}$ , the characteristic mass proportion of the dust and gas components  $\rho_{d0}/\rho_{g0} \approx 0.01$ , and the speed of sound in the gas  $c_{s0} \approx 10^5 \text{ sm s}^{-1}$ , the characteristic optical depth  $\tau_0$  takes on values from 120 to 12 000. In our calculations we assumed  $\tau_0 = 120$  both for graphite and silicate particles.

Other dimensionless parameter, which we further call *radiative number*,

$$R = \frac{4\pi\sigma_{SB}m_g^3 c_{s0}^6}{\gamma^4 k_B^4 n_{g0} c}, \quad (34)$$

characterizes the relative contribution of the radiation pressure force. By definition, this parameter is the ratio of the radiation energy in a cylinder of a height equal to the mean free path of a photon  $l_{\text{ph}}$  to the thermal energy in a cylinder of a height equal to the Jeans length  $\lambda_J$ . The force of the radiation pressure depends on the mean free path. If  $l_{\text{ph}} > z_h$ , where  $z_h$  is the halfwidth of the cloud, which actually equals

to the Jeans scale, then the radiation freely escapes the medium not making a force impact on the cloud matter. With  $l_{\text{ph}}$  smaller than the cloud halfwidth, the radiation will exert force pressure on the matter, which is determined by the collisions of the photons and particles of the medium. Notice that the radiative number  $R$  can be expressed in terms of the radiation Boltzmann number  $\text{Bo}$  known from the heat transfer theory, which determines the role of convective energy transfer in the direction of the flow compared to the radiative energy transfer [43]:

$$R = \frac{4\pi}{c} \frac{c_{\text{s}0}}{\gamma - 1} \frac{1}{\text{Bo}}. \quad (35)$$

If one assumes the characteristic temperature  $T_0 = 100$  K, the gas concentration in the aforementioned range  $10^2$ – $10^6$   $\text{cm}^{-3}$ , and the gas particle mass to be  $m_{\text{g}} = 1.67 \times 10^{-24}$  g, then the radiative number  $R$  will be within the range of  $10^2$  to  $10^6$ .

The parameter characterizing the source of radiation is the flux of a source located in the origin of coordinates, normalized to the thermal energy flux radiated from some surface with a temperature  $T_0$ :

$$\tilde{F}_0 = F_0 / \sigma_{\text{SB}} T_0^4. \quad (36)$$

Dimensionless radiation flux from the source  $\tilde{F}_0$  was selected in such a way so that the contribution of the summand with the radiation pressure  $\tau_0 R \tilde{\alpha} \tilde{H} / \tilde{\rho}_{\text{d}}$  in the dynamic balance equation was approximately 1–100. Otherwise, either the radiation pressure is small, and then the dynamical effect of the radiation is accidental and the model under consideration is no more of interest, or the pressure is so great that a stationary state of equilibrium is missing. For the dimensionless flux  $\tilde{F}_0 = 2 \times 10^{-3}$  which is typical in our calculations, expressed in terms of dimensional values over a double-sided area of  $1 \text{ pc}^2$  on the source plane, we obtain a source luminosity of the order of  $5 \times 10^4 L_{\odot}$ . In other words, calculation of the planar source luminosity implies integration over a thin layer surrounding the plane of sources.

Let us estimate the order of another dimensionless parameter of the problem, the dust flux  $\tilde{Q}_{\text{d}}$ . For the accepted ratio between the dust and gas masses and the initial speed of sound  $c_{\text{s}0}$ , we obtain  $Q_{\text{d}} \approx 0.01$ . The rate of the dust outflow from the source  $\tilde{v}_{\text{d}0}$  is also a free parameter of the model. In the calculations, it was set of the order of unity.

We make the friction coefficient  $\beta$  dimensionless by dividing it by the characteristic dynamical time of the problem

$$t_{\text{dyn}} = \frac{\lambda_{\text{J}}}{c_{\text{s}0}} = (4\pi G m_{\text{g}} n_{\text{g}0})^{-1/2} \quad (37)$$

$$\simeq 0.845 \times 10^{14} \left( \frac{n_{\text{g}0}}{10^2 \text{ cm}^{-3}} \right)^{-1/2} \text{ s}.$$

The dust grain mass  $m_{\text{d}}$  included into determination of the friction coefficient (22) can be calculated in the following way:

$$m_{\text{d}} = \frac{4}{3} \pi a^3 \rho_{\text{grain}}$$

$$\simeq 9.34 \times 10^{-15} \left( \frac{a}{0.1 \text{ }\mu\text{m}} \right)^3 \left( \frac{\rho_{\text{grain}}}{2.23 \frac{\text{g}}{\text{cm}^3}} \right) \text{ g}. \quad (38)$$

The dust grain density  $\rho_{\text{grain}}$  usually varies in the range of 1.8–3.5  $\text{g}/\text{cm}^3$  [31]. In our model, we choose the value which is characteristic of a graphite particle and is equal to 2.23  $\text{g}/\text{cm}^3$ . We determine  $\tilde{\beta}$  from (22) using (37) and (38):

$$\tilde{\beta}(\tilde{z}, \tilde{v}_{\text{d}}) \equiv \beta t_{\text{dyn}}$$

$$= \tilde{\beta}_0 \tilde{\rho}_{\text{g}}(\tilde{z}) \tilde{c}_{\text{s}}(\tilde{z}) \left( \frac{a}{0.1 \text{ }\mu\text{m}} \right)^{-1} \left( 1 + \left( \frac{\tilde{v}_{\text{d}}(\tilde{z})}{\tilde{\zeta} \tilde{c}_{\text{s}}(\tilde{z})} \right)^2 \right)^{\frac{1}{2}},$$

$$\tilde{\zeta} = \frac{8\sqrt{2}}{3\sqrt{\pi\gamma}}, \quad (39)$$

where the coefficient  $\tilde{\beta}_0$  is actually one of the control parameters of the model and is equal to

$$\tilde{\beta}_0 \simeq 77.9 \left( 1 + \xi \right) \left( \frac{n_{\text{g}0}}{10^2 \text{ cm}^{-3}} \right)^{1/2}$$

$$\times \left( \frac{c_{\text{s}0}}{10^5 \frac{\text{cm}}{\text{s}}} \right) \left( \frac{\rho_{\text{grain}}}{2.23 \frac{\text{g}}{\text{cm}^3}} \right)^{-1}. \quad (40)$$

In those cases when influence of the friction coefficient on the character of the flow is investigated, we vary the parameter  $\xi$ , which determines the Coulomb friction contribution into the entire friction force, in the range of 0–3, and set it equal to zero in all other cases.

As a result, we have six dimensionless control parameters of the model:  $\tau_0$ ,  $R$ ,  $\tilde{F}_0$ ,  $\tilde{Q}_{\text{d}}$ ,  $\tilde{v}_{\text{d}0}$ , and  $\tilde{\beta}_0$ . Setting  $\tau_0$  and  $R$  from (28), (29), (33), and (34), we find the normalization constants  $n_{\text{g}0}$  and  $c_{\text{s}0}$ , and reconstruct  $T_0$  and  $\rho_{\text{g}0}$  from (26).

### 3.2. Boundary Conditions

The whole system of equations (30)–(31) is divided into two subsystems: hydrodynamic (30) and optical (31). For the hydrodynamic subsystem, we solve a Cauchy problem with the following boundary

conditions in the origin of coordinates:

$$\begin{aligned} \tilde{\rho}_g(\tilde{z} = 0) &= 1, & \tilde{\rho}_d(\tilde{z} = 0) &= \frac{\tilde{Q}_d}{\tilde{v}_{d0}}, \\ \tilde{v}_d(\tilde{z} = 0) &= \tilde{v}_{d0}, \\ \tilde{\Phi}(\tilde{z} = 0) &= 0, & \frac{d\tilde{\Phi}}{d\tilde{z}}(\tilde{z} = 0) &= 0. \end{aligned} \quad (41)$$

For the optical system, we solve a boundary value problem with boundary conditions (2) and (3).

The condition  $\tilde{T}(\tilde{z} = 0)$  is not laid on temperature. We calculate the temperature distribution with height including the temperature in the origin of coordinates, by means of iteration, solving both subsystems together (see next subsection). The pressure at the point  $\tilde{z} = 0$  is calculated with the formula

$$\tilde{P}(\tilde{z} = 0) = \frac{1}{\gamma} \tilde{T}(\tilde{z} = 0). \quad (42)$$

### 3.3. Calculation Procedure

In the calculation model, the two sources of heating radiation are considered: a point source located in the origin of coordinates and corresponding to the star radiation and a background radiation source distributed along  $\tilde{z}$  and maintaining the equilibrium temperature  $\tilde{T}_b = 0.1$  in the whole cloud in the absence of a point source.

In general, temperature distribution which provides the equilibrium is not known in advance. Thus, using some initial approximation of temperature distribution, let us plot the relation  $\tilde{T}(\tilde{z})$  so that the radiation field will satisfy energy balance equation (14) by means of iteration. As an initial distribution for the iterations, we assign  $\tilde{T}(\tilde{z}) = \tilde{T}_b$ .

Specifically, the calculation procedure reduces to the following. For some initial temperature distribution approximation, in the absence of a radiation source we solve hydrodynamic subsystem (30), from which we find the distribution of dust and gas densities. Using the obtained densities, we find optical parameters of the problem for an inhomogeneous medium: the optical depth  $\tau_i$  and the albedo of a single scattering  $\omega_i$  in a layer with the coordinates  $[\tilde{z}_i, \tilde{z}_{i+1}]$ . For the obtained parameters, we solve the radiation transfer equation in the  $\delta$ -Eddington approximation [34, 44, 45] and find the temperature anew from the radiative equilibrium equation. Upon that, the iteration process is repeated until the temperature distribution converges to some steady one (see Fig. 1).

The condition for the termination of the iteration process is a small value of misclosure, which is determined through the difference between temperature

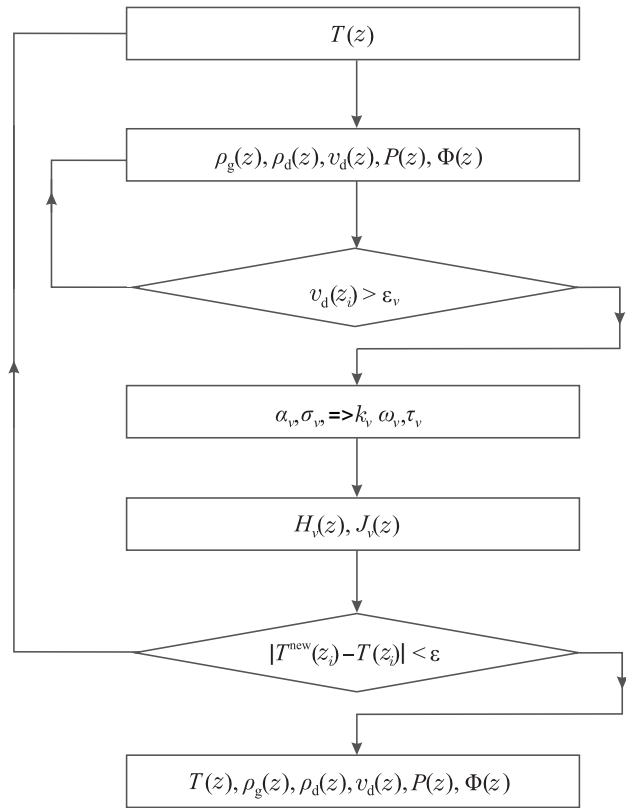


Fig. 1. Iteration procedure of solution of radiative hydrodynamics equation system of (30)–(31).

distributions in two neighboring iterations,  $n$  and  $(n + 1)$ :

$$\xi^n = \frac{\sum_{i=1}^N |\tilde{T}^{n+1}(\tilde{z}_i) - \tilde{T}^n(\tilde{z}_i)|}{\sum_{i=1}^N |\tilde{T}^n(\tilde{z}_i)|}. \quad (43)$$

Iterations are repeated until the condition  $\xi \leq \epsilon_\xi$  is satisfied, where  $\epsilon_\xi$  is some preset accuracy. In our calculations, we confined ourselves to the accuracy  $\epsilon_\xi = 10^{-4}$ .

The motion of dust as a collisionless medium allows the possibility of multiple flows emerging near the turning points. In our model, as shown in Section 4, that dust motion is found steady in which interpenetrating flows are formed, converging to the dust accumulation layer.

In the present paper, we confine ourselves to consideration of an transitional stage when the return flows have not been formed yet, and in this case the dust motion can be considered as single-flow. Thus,

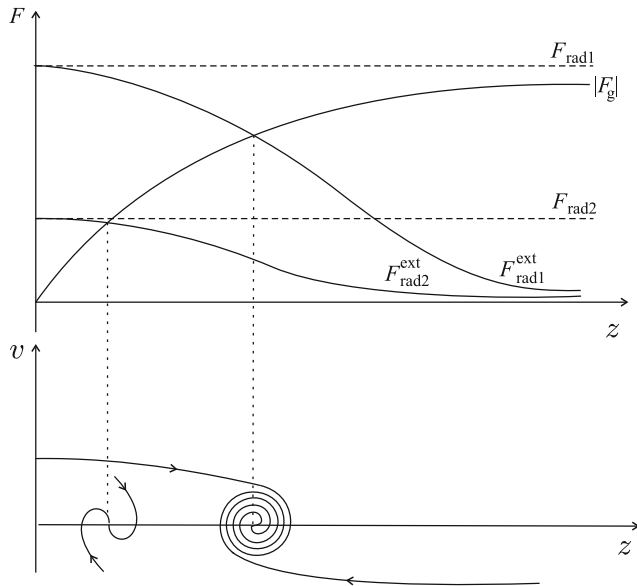


**Fig. 2.** Diagram of the distributions of the gravitational force  $F_g$  and the radiation pressure force  $F_{\text{rad}}$  with height  $z$  (upper figure). The radiation source is in the origin of coordinates. The dashed lines  $F_{\text{rad}1}$  and  $F_{\text{rad}2}$  show the radiation pressure forces for the medium with a negligible concentration of dust, and the solid curves  $F_{\text{rad}1}^{\text{ext}}$  and  $F_{\text{rad}2}^{\text{ext}}$ —for the case of a finite concentration. Stable equilibrium points on the phase plane correspond to the crossing of the curves (lower figure).

here we describe the dust as a single-fluid and single-velocity continuum.

In every iteration temperature step, an additional condition of a breakpoint is laid in the hydrodynamic block, corresponding to approaching the first turning point  $\tilde{z}_T$  in the dust flow, in the vicinity of which the condition  $|\tilde{v}_d| \leq \varepsilon_v$  is fulfilled. As soon as this inequality is satisfied, the calculation in the hydrodynamic block is terminated. We accepted  $\varepsilon_v = 10^{-2}$  in our calculations.

The calculation can be continued beyond the first turning point. In this region, the gas is in equilibrium maintained by the forces of proper pressure and gravitation. Since the gas is transparent for radiation when there is no dust, and does not radiate itself, it is not necessary to calculate its temperature distribution and we consider it isothermal.

## 4. RESULTS OF NUMERICAL MODELLING

### 4.1. Structure of the Flow: Qualitative Scheme, Turning and Equilibrium Points

Two special states of dust particle motion in the medium can be distinguished from all the possible. In the turning point, the velocity of a dust grain is

zero and the acceleration is different from zero. In the equilibrium state (the accumulation point), both velocity and acceleration vanish simultaneously. The location of the turning points is defined by the law of particle motion and can not be determined from the comparison of the effect of forces only. To find a turning point, it is needed to integrate the whole system of differential equations. Conversely, the presence or absence of equilibrium points and their location can be determined by comparing only two forces which do not depend on dust particle velocity: the gravitational force and the force of radiation pressure.

The geometry of the problem is such that the gravitational force monotonously grows with height  $z$  as the entire gravitational mass of the cloud accumulates in the interval from 0 to  $z_h$  and asymptotically reaches the constant value  $|F_g(\infty)|$  (the curve  $|F_g|$  in Fig. 2), because the mass in every vertical cross-section of the cloud is finite. In the extreme case, when the dust concentration is vanishingly small and the dust does not cause shielding of the radiation, the radiation pressure force, affecting every dust particle, is constant in height (the dashed lines  $F_{\text{rad}1}$  and  $F_{\text{rad}2}$  in Fig. 2). Two cases are possible then depending on the relation between  $F_{\text{rad}}$  and  $|F_g(\infty)|$ . In the case  $F_{\text{rad}} > |F_g(\infty)|$ , the example of which is the dashed straight line  $F_{\text{rad}1}$  with no intersection points with the curve  $|F_g|$  (see Fig. 2), the dust particle escapes to infinity even in the presence of friction. If  $F_{\text{rad}} < |F_g(\infty)|$ , then the curves  $F_{\text{rad}2}$  and  $|F_g|$  in Fig. 2 will have an intersection point, which corresponds to the equilibrium state. It can be seen from the figure that the difference of forces which arises when a dust particle deviates from the equilibrium state is of a restoring force character and, consequently, this equilibrium state is stable. If we take the dust final concentration into account now, the shielding effect will result in the fact that the radiation force will decrease monotonously with height. Then, the final distribution of concentration will be found, at which the curves corresponding to the radiation pressure force and gravitational force will have an intersection point ( $F_{\text{rad}1}^{\text{ext}}$  and  $|F_g|$  in Fig. 2). The friction force does not affect the fact of the presence of equilibrium and the location of equilibrium points but can change the kind of the critical point. With friction force increase, a stable focus converts into a stable node. Figure 2 (at the bottom) shows both types of the critical points.

### 4.2. Characteristic Time Scales. Calculation of the Flow Structure in the Single-Flow Approximation

The flow can be considered stable when the flow parameters (velocity, concentration) in every point  $z$  do not change with time. In the presence of the

accumulation layer, the flow can be stable everywhere outside this layer, while the dust concentration grows with time in the layer itself. Transition to a stable flow takes formally infinite time; however, during this process several stages can be separated out, each of which exhibits its own time. The dynamical time  $t_{\text{dyn}}$ , which we determine as the time of the dust grain motion from the source to the first turning point, characterizes the transitional stage, at which the dust cocoon forms. For the characteristic values of dust velocity in our problem  $v_d \sim 4\text{--}6 \text{ km s}^{-1}$  and the cocoon scale  $z_T \sim 0.2\text{--}6 \text{ pc}$ , where  $z_T$  is the coordinate of the first turning point, we have  $t_{\text{dyn}} \sim 3 \times 10^4\text{--}1.5 \times 10^6 \text{ yr}$  as the dynamical time. Thus, at times of the order of fractions of million years, the primary flow of the outflow from the source inside the cocoon forms, but the flow itself stays single-flow. At times greater than dynamical, the reverse flows emerge, a region of multiple flows (a shell) and an accumulation layer inside the shell are gradually forming. The flow can be roughly considered stable if the mass  $m_{\text{env}}$  of the dust accumulated in the shell is much greater than the mass of the dust in the primary flow  $m_{\text{prim}}$ . The corresponding time of relaxation to the steady state is, consequently,  $t_{\text{rel}} \sim \frac{m_{\text{env}}}{m_{\text{prim}}} t_{\text{dyn}} \gg t_{\text{dyn}}$ . We consider the transitional stage.

It can be predicted, however, that the multiflowness in the shell and settling of the dust in the layer would result in a situation where the dust completely shields the radiation out of the accumulation layer. It means that the turning point on the outer edge of the shell should approach the accumulation point, and the shell will be narrower at the relaxation stage than that at the transitional stage, which we calculate here.

#### 4.3. Vertical Structure of the Gas and Dust Cloud for Different Parameters of the Model. Numerical Calculations

The most physically significant dynamical and thermal effects of the interaction between heating radiation and matter manifest themselves in the conditions when such an interaction is great. The heating will be considerable when the true absorption of the UV radiation by the dust  $\tilde{k}/\tilde{\rho}_d$  is more intense than the absorption of the proper radiation of the dust grain  $\tilde{k}_*/\tilde{\rho}_d$ . Figure 3 shows that in our model this condition is fulfilled for the whole acceptable range of dust grain sizes. Apart from that, the condition of the validity of the considered model is the required transparency of the medium to the proper cooling radiation of the dust. Figure 3 also shows that it is important to take scattering into consideration, as it makes the contribution which is approximately equal

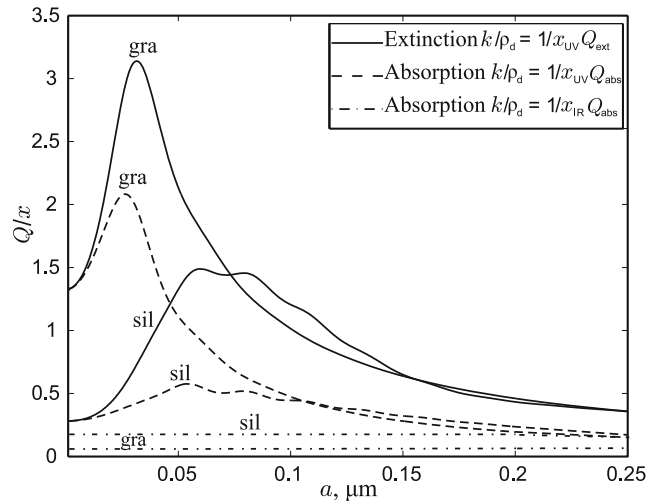


Fig. 3. Dependences of the opacity on the particle size for graphite and silicate particles.

to the contribution of the absorption into the entire attenuation of radiation by the medium.

At first, let us consider the dependence of the flow structure on the dust particle size (Fig. 4). The radii of the dust particles varied from  $a = 0.05$  to  $0.15 \mu\text{m}$  in increments of  $0.05 \mu\text{m}$ .

The following features of the flow can be distinguished qualitatively. Influenced by the radiation pressure force, which dominates other forces in the central regions of the cloud (Figs. 4e and 4f), dust particles accelerate to great speeds, which in some parts of the flow are equal to more than ten speeds of sound (Fig. 4c) and sweep out the gas from the central regions (Fig. 4b). A heated cavity, which is both gas and dust depleted, is left in the center of the cloud. With distance from the center, the dust grains decelerate because of the friction, the radiation pressure force due to the shielding by the dust, and also because of the increasing gravitational force, and finally they stop at some point with the coordinate  $\tilde{z}_T$  and turn back.

At the initial stage, at distances  $z \sim 0.2 \text{ pc}$  from the center, in the regions where gas concentration is high (see Fig. 4b), the dust is overdamped (i.e., the approximate equation of the accelerating force of the radiation pressure and the decelerating gravitational force is fulfilled, Figs. 4e and 4f) and moves with a relatively small acceleration. Upon the emission of the gas from the gaseous cocoon at  $z > 0.2 \text{ pc}$ , it becomes rarified and, correspondingly, the friction force abruptly decreases. Still, the gravitational force is not big enough to resist the radiation pressure, and the dust particle accelerates fast. Optical parameters for dust grains with sizes  $a = 0.1$  and  $0.15 \mu\text{m}$  are such that the acceleration  $\tilde{f}_{\text{rad}}$  created by the radiation

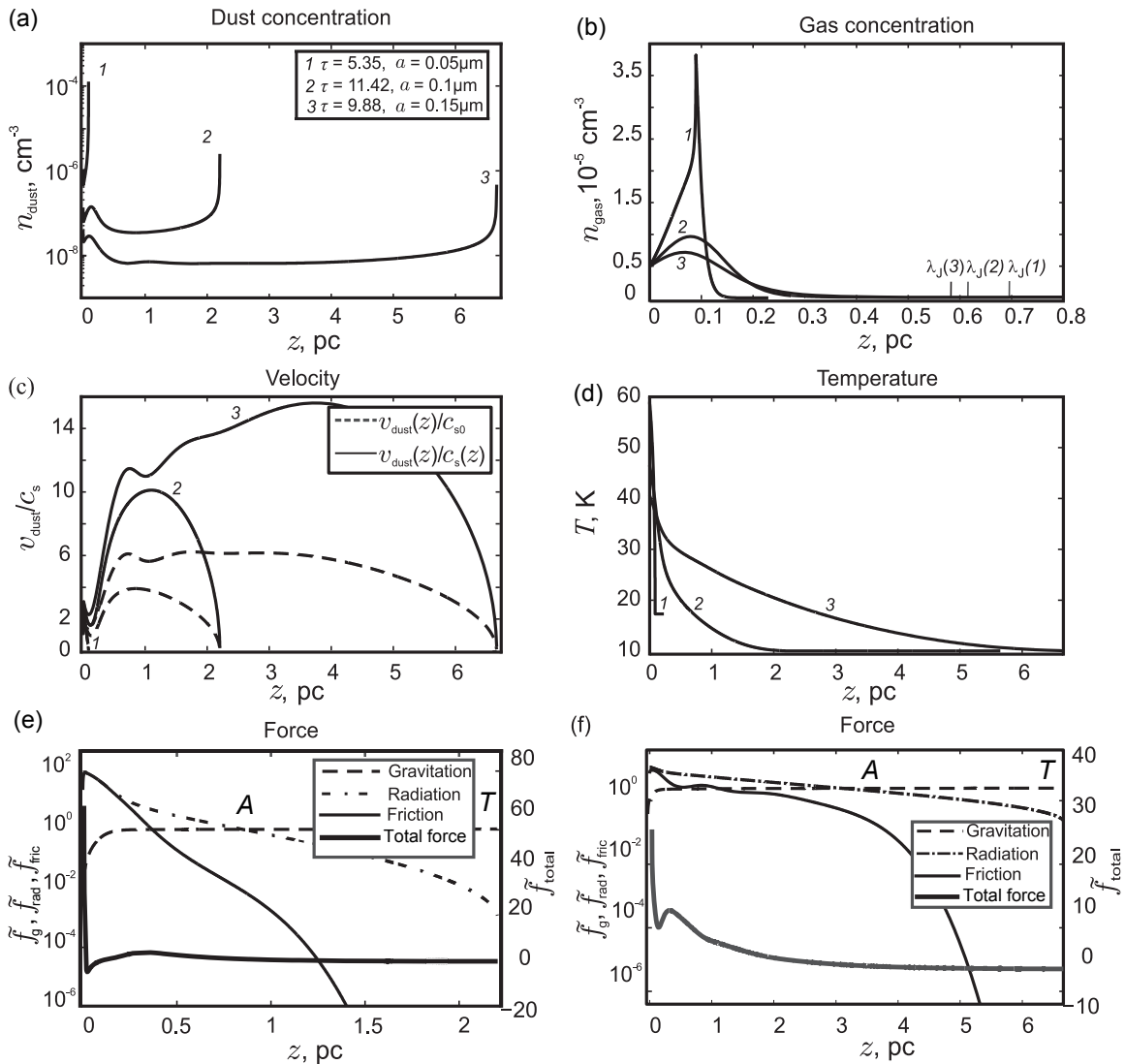


**Fig. 4.** Distributions with height  $z$ : (a) dust concentration; (b) gas concentration; (c) dust velocity normalized to the local speed of sound in the gas (solid curves) and also the absolute dimensionless dust velocity  $\tilde{v}_d$  (dashed curves); (d) temperature; (e) accelerations created by the gravitational ( $\tilde{f}_g$ , dashed curve), friction ( $\tilde{f}_{\text{fric}}$ , thin solid curve), and radiation pressure ( $\tilde{f}_{\text{rad}}$ , dash-dotted curve) forces, the determination of the accelerations is given in system (30), and also the total acceleration  $\tilde{f}_{\text{total}}$  (thick solid curve) which a dust particle undergoes, for distribution 2; (f) the same for distribution 3. In the point of the balance of the radiation pressure force and gravitational force (the point A), the dust accumulation layer should set in. Radiation number  $R = 2 \times 10^3$ , coefficient  $\beta_0 = 45$ , dust mass flux  $\tilde{Q}_d = 0.015$ , radiation flux  $\tilde{F}_0 = 2 \times 10^{-3}$ . The distributions are constructed for three different dust particle sizes. The distribution of gas concentration for model 1 is constructed in the region spreading beyond the turning point. The legend on panel (a) gives the optical depths  $\tau$  for all the three distributions. On panel (b), the values of the Jeans length  $\lambda_J$  are marked (see (29)) for all the three distributions.

pressure turns out higher for the bigger dust grains. Consequently, big dust grains accelerate faster, and due to the dust-mass flow conservation in the dust cocoon, the concentration of them is lower than that of the small dust grains, they shield the radiation weaker because of that and move away for long distances.

With the relaxation to the steady-state, the dust in the cloud will form the structure similar to a cocoon

with the halfwidth  $\tilde{z}_T$ , in which the main mass of the dust will be concentrated in the shell in the region of reciprocating movements between the first two turning points.

Finally, the dust particles should accumulate in the point A, which is the balance of the gravitational force and the radiation pressure (see Figs. 4e and 4f), in the steady static equilibrium.

Since we consider the early stage of the cocoon

formation, and the reverse dust flows in the shell are not taken into consideration, the contribution of the shell to the shielding of the source radiation at big  $\tilde{z}$  is underestimated, which means that the cocoon is too stretched at this transitional stage of the flow. As the shell forms at the stage of relaxation to the steady flow, the  $\tilde{z}_T$  and  $\tilde{z}_A$  values will decrease. Thus, the dust cocoon size  $\tilde{z}_T$  and the height  $\tilde{z}_A$  of the accumulation point in the numerical calculations of the present paper should be taken as upper estimates.

The gas as well as the dust forms the distribution with a dip of density in the center and a maximum at some finite height. Though, compared to the dust, the density gradients in the gas cocoon are not so big; along with this, the cavity originating in the gas and the gas shell have approximately similar sizes. As a halfwidth of the gas layer, it is natural to assume such a height  $\tilde{z}_h$  which contains the main mass of the gas (for instance, 99% of the total amount) within the interval  $[-\tilde{z}_h, \tilde{z}_h]$ . Then two different configurations are possible, when the halfwidth of the dust cocoon  $\tilde{z}_T$  in the cloud either coincides with the halfwidth of the gas layer (curve 1) or exceeds it (curves 2 and 3). Moreover, the difference in scales can reach big values, 10–30 times. In this case, in the profile of the dust shell, the density peak can be distinctly visible in the region of the gas shell location.

Notice that in Fig. 4 we provide gas concentration distributions stretching beyond the boundaries of the dust cocoon, further we confine ourselves to presenting the distributions inside the cocoon only.

The most physically interesting effect appearing from Fig. 4, in our opinion, is the inverse gas distribution with height, by which we mean such a distribution when a colder heavy fluid is in the field of gravity above a heated and lighter fluid. With such a distribution, the gas entropy  $S \sim \ln(T/\rho^{\gamma-1})$  decreases with height and, in accordance with the Schwarzschild criterion, is convectively unstable [46]. However, the medium considered in our model is an open system due to the interaction of the dust component with the external radiation, and therefore it is not correct to apply the Schwarzschild criterion to this system. Although, if one takes into consideration a real multidimensional cloud and accepts that owing to one or another dynamical processes the dust can inhomogeneously redistribute along the directions perpendicular to the height of the cloud, then it can be noticed that the conditions for the emergence of convective instability should occur. Let us assume that the dust from some column of the gas is completely transferred to a neighboring gas column. Then the initial gas column will become completely transparent to the radiation, lose its supporting dust friction force and the equilibrium, and, consequently, begin to contract in height tending to retrieve the equilibrium. With such

one-dimensional adiabatic contraction, the entropy of every gas particle preserves as well as the arrangement of the gas particles in height. It means that if initially  $dS/dz < 0$  at the equilibrium loss moment, then this inequality remains true as well after the transition of the gas to the equilibrium state, such a distribution is convectively unstable with certainty. Thus, in a more general multidimensional optical-dynamical model of the gas and dust cloud, we may expect development of convective motions. Moreover, we may expect the convection not to attenuate, as gas redistributions will not eliminate the cause of convective instability occurrence and the reasons for emerging the convection: the radiation from the source is kept permanent, and the dust cannot be carried beyond the cloud by the radiation pressure.

Notice that earlier we have discovered the convectively unstable distributions of the gas in a more particular model, in which the freezing-in of the dust in the gas was supposed [9]. This model corresponds to the extreme case  $\beta \rightarrow \infty$ ,  $Q_d \rightarrow 0$ . In the present model, the inverse distribution preserves as well with the finite friction coefficients, which can be seen both from Fig. 4 and from Fig. 5, which shows the distributions for different values of the friction coefficients.

The radiation parameter  $R$  characterizes the relative contribution of the radiation pressure force. Figure 6 shows that with the increase of  $R$  (this corresponds to the radiation pressure increase) and with all other conditions being equal, the turning point shifts toward the region of great heights, but the gas distribution is of low sensitivity to the  $R$  variations.

Figure 7 illustrates the influence of the radiation flux  $\tilde{F}_0$  from the source on the character of the distributions. With the increase of the radiation flux, the gas and dust are more strongly heated, at the same time the gradients in the gas concentration distribution slightly increase.

Figure 8 shows the distributions for different dust flux values. The diagrams demonstrate that the more dust is injected to the cloud by the source, the stronger the gas is entrained by the dust (curves 2 and 3). The outflows with little dust make more gradual distributions but the dust can be carried away to the cloud periphery. This is caused by the weaker shielding of the radiation by the dust.

Figure 9 shows that the initial velocity of the outflow is not an essential parameter in the model. The process of dust dispersion is practically inertialess, and the velocity field is determined by the balance of forces. The dust velocity at small initial distances (of the order of one hundredth of the dust cocoon size) is adjusted to the settled equilibrium distribution of velocity.

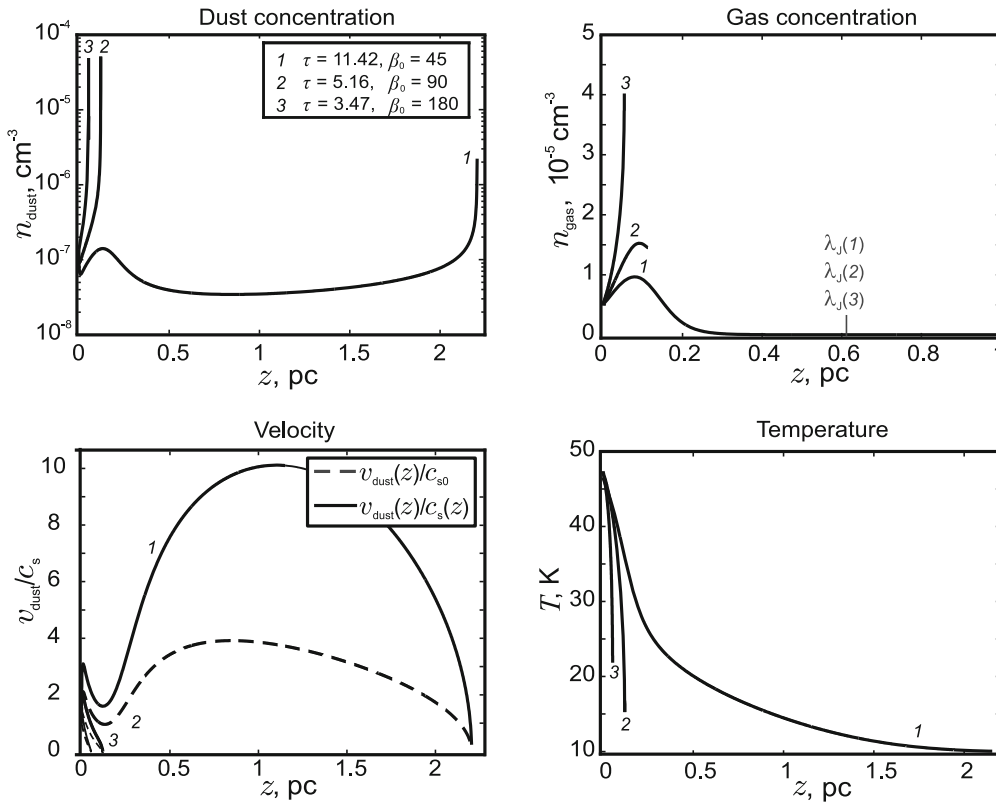


**Fig. 5.** Distributions with height  $z$  of the dust concentration (top left), gas concentration (top right), temperature (bottom right), and the dust velocity (bottom left) normalized to the local speed of sound in the gas (solid curves) as well as the absolute dimensionless dust velocity  $\tilde{v}_d$  (dashed curves). The radiation number  $R = 2 \times 10^3$ , dust mass flux  $\dot{Q}_d = 0.015$ , incident radiation flux  $\tilde{F}_0 = 2 \times 10^{-3}$ , dust particle size  $a = 0.1 \mu\text{m}$ . The distributions are constructed for three different values of  $\beta_0$ .

Finally, Fig. 10 demonstrates the different behavior of the graphite and silicate particles. The silicate particles, as dielectrics, interact with the radiation weaker than the graphite particles, which are of electrical origin similar to metals. Correspondingly, dust cocoons with silicate particles are more compact.

## 5. DISCUSSION AND CONCLUSIONS

In the present paper, we developed a hydrodynamic model of a self-gravitating gas and dust interstellar cloud threaded with the radiation of the stars located in its center. The model is based on the following assumptions:

- (1) the cloud consists of cold gas and cold dust with the characteristic temperatures in the range of 10–60 K;
- (2) dust particles interact with the radiation field of the stars located in the center of the cloud, and accelerate to supersonic speeds of 1–7 km s<sup>-1</sup> under the influence of radiation pressure;
- (3) the radiation transfer on the dust is taken into consideration and is calculated in the  $\delta$ -Eddington approximation;

(4) the dust is monodisperse;

(5) the gas is transparent to the radiation, its equilibrium is provided by the balance of the forces of the cloud self-gravity, gas pressure, and is supported by the friction force from the dust in motion;

(6) the dust is produced by the sources in the center of the cloud and moves from the center to the periphery, while the gas rests in the hydrostatic equilibrium.

Let us note the following general results of calculations.

(1) The key characteristic determining the structure of the gas and dust cloud threaded with the stellar radiation is the optical depth of the dust component.

If the dust is rarified and its optical depth is small, the radiation of the stars can sweep it outside the cloud. If dust concentration is high, a dust cocoon forms in the center of the cloud, i.e., a layer of a finite thickness in which all the dust contributed by the stellar sources is concentrated.

In the structure of the dust cocoon, we can distinguish three major structural elements, which are

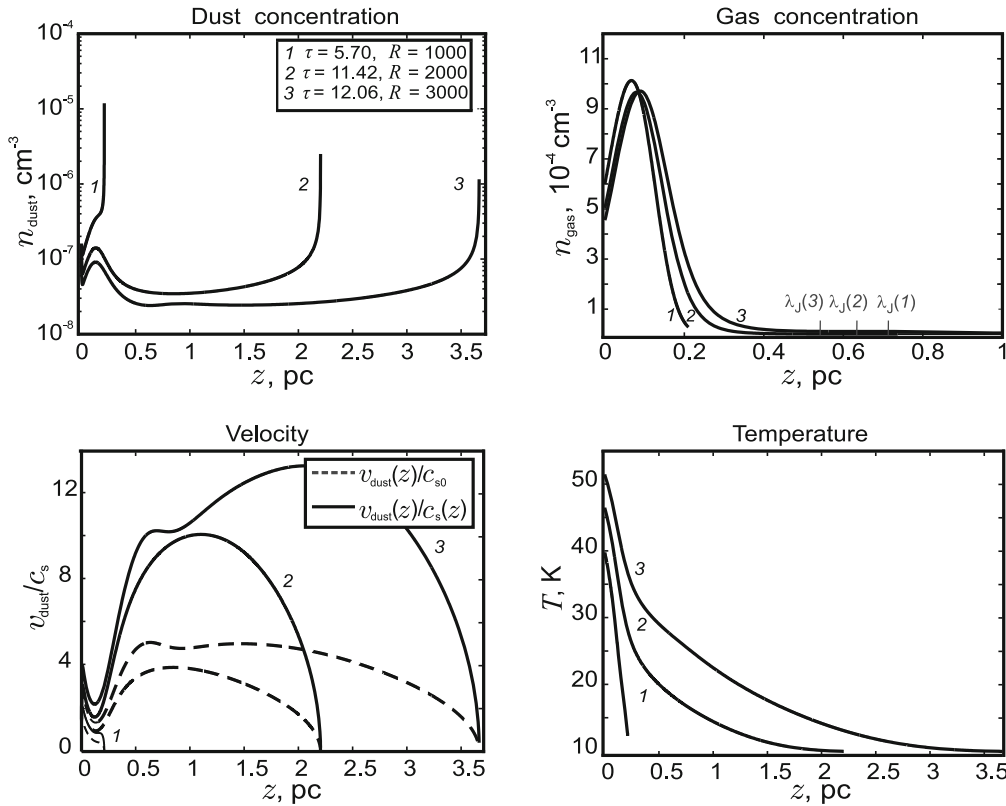


**Fig. 6.** Distributions of the dust concentration (top left), gas concentration (top right), temperature (bottom right), and the dust velocity (bottom left) normalized to the local speed of sound in the gas (solid curves) as well as the absolute dimensionless dust velocity  $\tilde{v}_d$  (dashed curves). The coefficient  $\tilde{\beta}_0 = 45$ , dust mass flux  $\tilde{Q}_d = 0.015$ , incident radiation flux  $\tilde{F}_0 = 2 \times 10^{-3}$ , dust particle size  $a = 0.1 \mu\text{m}$ . The distributions are constructed for three different values of the radiation number  $R$ .

characterized by the scale hierarchy. The first element, a cavity, is the inner part of the cocoon, embracing the spacial interval from the cocoon center to the shell and filled with dust and gas of low concentration. In this part of the cloud, a single-flow regime of the dust outflow from the cloud center to the periphery is realized. The characteristic sizes of the cavity are from several hundredths to tenths of a parsec depending on the parameters of the model. The cavity size can be both comparable by the order of magnitude to the size of the cocoon itself and much smaller than the cocoon.

The second structural element of the cocoon is a shell located near its surface and filled with dust with a concentration that is hundreds, thousands, and more times greater than the dust concentration in the cavity. Dust flows in the shell are multiple. The boundary separating the cavity and the shell is the point of the second turning in the dust flow, which is the closest one to the cocoon center of all the numerous turning points.

The characteristic thickness of the dust shell  $l_{\text{env}}$  is tenths of the cross-section size of the cocoon depending on the power of the dust wind or, if the wind is strong, the cocoon consists of the shell almost

completely. Although in the model corresponding to the steady multiple flows at the relaxation stage, we expect a considerable decrease of the shell size, as the contribution of the dense accumulating layer to the radiation shielding will be taken into consideration.

The third structural element is an infinitely thin layer, in which the dust deposits and, formally, the dust concentration in this layer becomes infinite. Physically the thickness of the accumulating layer will be small but not zero. The thickness is primarily restricted by the diffusive bleeding of the dust layer. Let us take into account the dust grain diffusion as an ensemble of Brownian particles, which has not been considered earlier. In the vicinity of the equilibrium point, the resultant of the two forces—self-gravitation and radiation pressure—has the character of a restoring force, which is linear in small shift  $\Delta z$  relative to the equilibrium position:  $\Delta F = -m_d \omega_0^2 \Delta z$ . Here  $\omega_0$  is the particle oscillation frequency in the vicinity of the equilibrium position, characterizing the degree of stiffness of the restoring force. In the stationary case, for the ensemble of particles the Boltzmann distribution settles:  $n_d \sim \exp(-m_d \omega_0^2 z^2 / 2k_B T)$ . It follows from here that the halfwidth of the particle

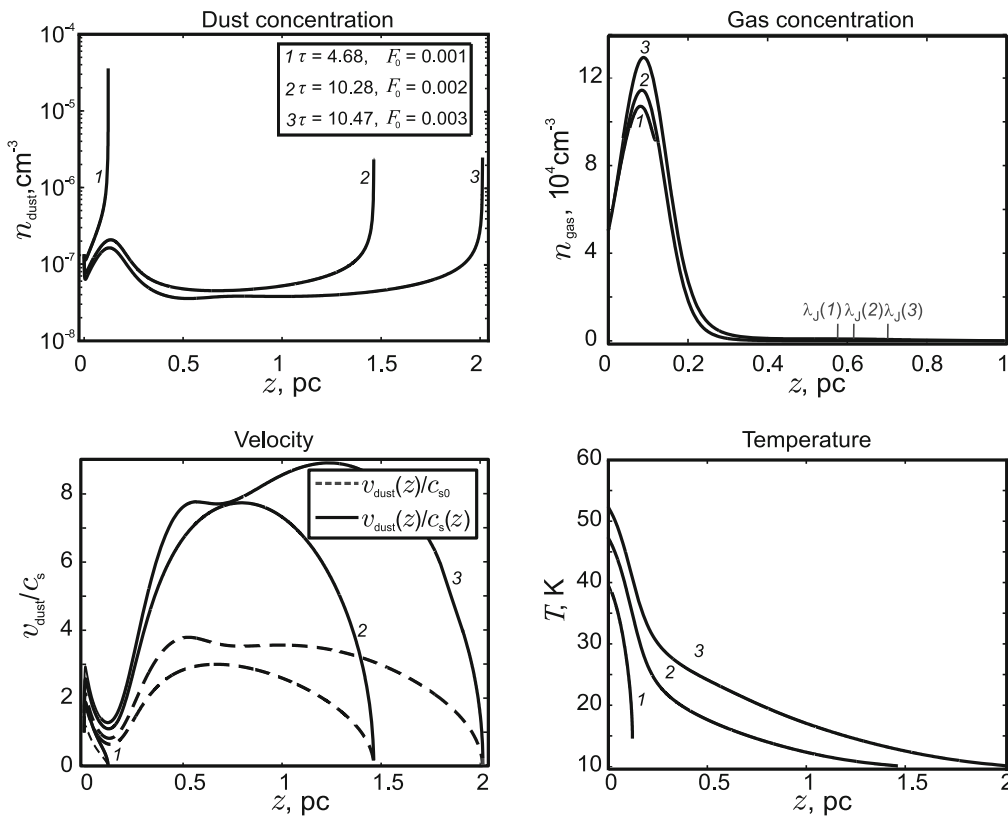


**Fig. 7.** Distributions of the dust concentration (top left), gas concentration (top right), temperature (bottom right), and the dust velocity (bottom left) normalized to the local speed of sound in the gas (solid curves) as well as the absolute dimensionless dust velocity  $\tilde{v}_d$  (dashed curves). The radiation number  $R = 1.2 \times 10^4$ , coefficient  $\tilde{\beta}_0 = 45$ , dust mass flux  $\tilde{Q}_d = 0.015$ , dust particle size  $a = 0.1 \mu\text{m}$ . The distributions are constructed for three different values of radiation flux  $\tilde{F}_0$ .

accumulation layer near the equilibrium position is equal to  $l_A = (2k_B T/m_d \omega_0^2)^{1/2}$ .

The table shows the numerical calculations for particles of different sizes for the distributions given in Fig. 4. It follows from the table that the thickness of the dust accumulation layer is  $l_A \approx 10^{-7}$  pc.

Finally, we have the following proportions:  $l_{\text{cav}} : l_{\text{env}} : l_A \approx 1 : \{1-30\} : \{10^{-7}-10^{-6}\}$ .

All three elements of the cocoon contain a finite mass of dust. In the model that we used, the dust is generated by the sources in the center of the cloud, passes through the cavity and shell, and finally settles

Parameters of the particle accumulation layer for the graphite particles

$a, \mu\text{m}$	$T, \text{K}$	$\omega_0, \text{s}^{-1}$	$l_A, \text{pc}$
0.05	17.3	$83 \times 10^{-12}$	$0.44 \times 10^{-7}$
0.1	15.8	$1.8 \times 10^{-12}$	$4.8 \times 10^{-7}$
0.15	16.1	$1.0 \times 10^{-12}$	$1.2 \times 10^{-7}$

in the accumulation layer. In the approximation of a stationary flow, the masses of the dust in the cavity and shell are permanent, and the mass of the dust in the accumulation layer grows with time. The latter formally contradicts the assumption on the stationarity of the flow, although at the times when the mass of the dust in the accumulation layer stays small compared to the mass of the dust in other parts of the cocoon, the variation of this mass can be neglected, and then the stationary approximation is justified. The second condition of the applicability of the stationary model is the slowness of the process of dust accumulation in the accumulation layer in comparison with the characteristic time of the flow relaxation to the settled regime.

(2) All the stated conclusions concerning the cocoon structure also remain valid for the model of a cloud with the more realistic spherical geometry. Actually, the presence or absence of the accumulation point and its spacial position are determined by the balance of the gravitational and radiation pressure forces. In the planar geometry, both forces have similar asymptotics at infinity (approach to a constant), and the balance is mainly determined only by the

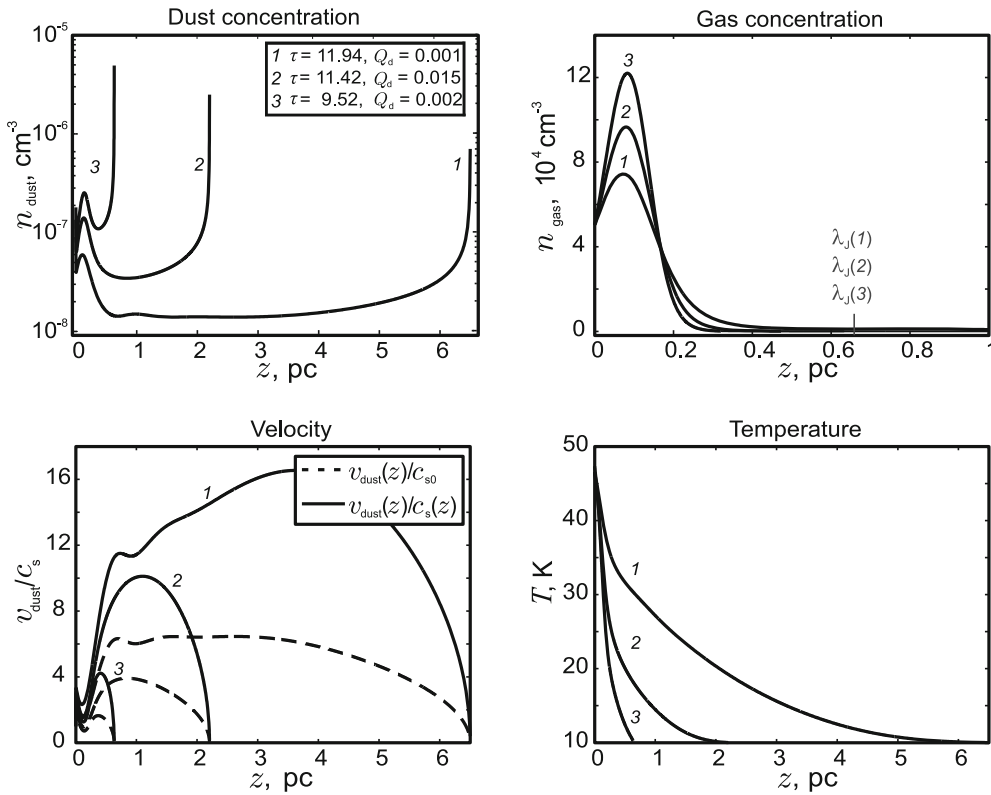


**Fig. 8.** Distributions of the dust concentration (top left), gas concentration (top right), temperature (bottom right), and the dust velocity (bottom left) normalized to the local speed of sound in the gas (solid curves) as well as the absolute dimensionless dust velocity  $\tilde{v}_d$  (dashed curves). The radiation number  $R = 2 \times 10^3$ , coefficient  $\tilde{\beta}_0 = 45$ , incident radiation flux  $\tilde{F}_0 = 2 \times 10^{-3}$ , dust particle size  $a = 0.1 \mu\text{m}$ . The distributions are constructed for three different values of dust flux  $\tilde{Q}_d$ .

relation between these asymptotic constant values of the forces. In the spherical geometry, both forces will decrease with distance according to the inverse square law, and thus the balance of the forces will as well mainly be determined only by the relation between constant multipliers of these asymptotic dependences. Along with this, however, owing to weakening of the forces with distance in the spherical geometry, the dust particle acceleration and, correspondingly, the cocoon sizes will turn out smaller than those in the present planar model. On the other side, to escape the gravity well in the spherical case, the dust particle needs to break a potential barrier of a finite height, while in the planar case the potential barrier height is infinite. Thus, in the spherical case, the dust wind with the dust outflow to infinity is possible, while in the planar case the dust occurs to be closed inside the cocoon.

(3) Infinite dust concentration values in the turning points and accumulation layer, which are obtained within the present model framework, are determined by the specific character of the dust component monodispersity approximation. Actually, the dust is polydisperse, and dust particles of different sizes will

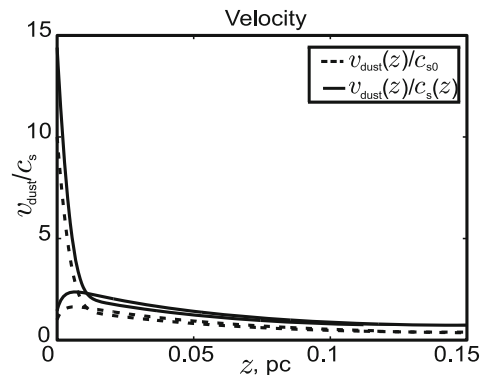


**Fig. 9.** Distributions of the dimensionless absolute  $\tilde{v}_d$  (dashed line) and relative  $v_d/c_s$  (solid line) velocities for two different initial velocities  $v_{d0}$ . The radiation number  $R = 2 \times 10^3$ , dust mass flux  $\tilde{Q}_d = 0.015$ , radiation flux  $\tilde{F}_0 = 2 \times 10^{-3}$ , dust particle size  $a = 0.1 \mu\text{m}$ , coefficient  $\tilde{\beta}_0 = 70$ . The turning point is located beyond the figure and has the coordinate  $\tilde{z}_T = 0.46 \text{ pc}$ .

turn/accumulate in different points throughout the height of the cloud. As a consequence, in the shell a smooth distribution of dust concentration will be

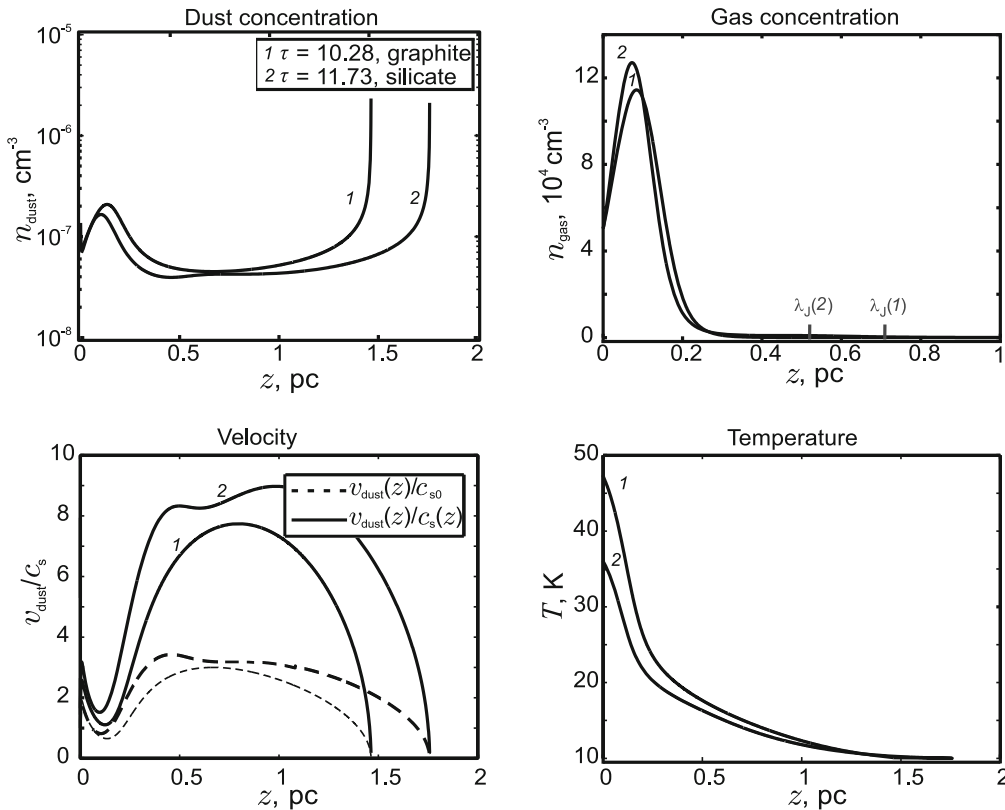


**Fig. 10.** Distributions of the dust concentration (top left), gas concentration (top right), temperature (bottom right), and the dust velocity (bottom left) normalized to the local speed of sound in the gas (solid curves) as well as the absolute dimensionless dust velocity  $\tilde{v}_d$  (dashed curves) for the silicate (curve 2) and graphite (curve 1) dust particles. The radiation number  $R = 2 \times 10^3$ , coefficient  $\tilde{\beta}_0 = 45$ , radiation flux  $\tilde{F}_0 = 2 \times 10^{-3}$ , dust mass flux  $\tilde{Q}_d = 0.015$ , dust particle size  $a = 0.1 \mu\text{m}$ .

observed instead of sharp peaks. Moreover, it is obvious that the spacial variations in the dust particle distribution by sizes will appear in the cloud. This conclusion can be proved with observations. A similar dust particle distribution by sizes is observed in the Galaxy disk [47], which is possibly determined by dynamical processes, e.g., by the influence of spiral arms. More detailed observations allow us to notice specific features of such distributions: particle sizes grow toward the edge of the Galaxy [48] and with distance from the disk plane [49], and this agrees with what we obtain in our model (Fig. 4).

(4) The picture will be more complicated if we take into account the actual non-one-dimensionality of the flow. According to simple qualitative reasoning given in Section 4.2, the gas and dust cocoon with the inverse distribution of gas density and temperature, which we obtained from our calculations, should be convectively unstable and, consequently, with the development of instability its structure will be reorganized. In particular, the thin dust shell and all the more the accumulation layer will be converted into a vortex pall extended in thickness and with distribution profiles of average concentrations strongly smoothed

along the vertical coordinate. If our assumption on the development of instability in the cloud in the case of inverse gas distributions under the influence of dust wind turns out to be right, then one can expect that the turbulence origin in gas and dust interstellar clouds on a scale of parsecs and subparsecs can be explained with this mechanism. The two-dimensional numerical calculations of non-stationary flows of stellar wind in dust circumstellar shells, indicating the development of instability similar to convective, count in favor of this assumption [15, 17, 18].

#### ACKNOWLEDGMENTS

The study has been conducted in the framework of the projects supported by the Russian Foundation for Basic Research (grants 11-02-01332a and 15-42-02682-r-povolzhie\_a). A. M. Zankovich is grateful to the Dynasty Foundation for financial support. The authors thank the referee for their useful comments.

#### REFERENCES

1. M.-M. Mac Low and R. S. Klessen, *Rev. Modern Physics* **76**, 125 (2004).

2. B. Elmegreen, *Astrophys. J.* **577**, 206 (2002).
3. E. A. Bergin and M. Tafalla, *Annual Rev. Astron. Astrophys.* **45**, 339 (2007).
4. E. Vazquez-Semadeni, arXiv:1202.4498.
5. A. Burkert, *Comptes Rendus Physique* **7**, 433 (2006).
6. N. Schneider, Ph. André, V. Könyves, et al., *Astrophys. J.* **766**, L17 (2013).
7. A. Brandenburg and Å. Nordlund, *Reports on Progress in Physics* **74**, 046901 (2011).
8. N. G. Bochkarev, *Foundations of the Physics of the Interstellar Medium* (Librokom Publ., Moscow, 2010).
9. E. V. Zhukova, A. M. Zankovich, I. G. Kovalenko, and K. M. Firsov, *Vestnik Volgograd. gos. univer., Ser. 1, Matematika, Fizika, No. 1(16)*, 57 (2012).
10. D. Krüger, A. Gauger, and E. Sedlmayr, *Astron. and Astrophys.* **290**, 573 (1994).
11. D. Krüger and E. Sedlmayr, *Astron. and Astrophys.* **321**, 557 (1997).
12. N. Mastrodomos, M. Morris, and J. Castor, *Astrophys. J.* **468**, 851 (1996).
13. S. Höfner, M. U. Feuchtinger, and E. A. Dorfi, *Astron. and Astrophys.* **297**, 815 (1995).
14. Y. J. W. Simis, V. Icke, and C. Dominik, *Astron. and Astrophys.* **371**, 205 (2001).
15. P. Woitke, *Astron. and Astrophys.* **452**, 537 (2006).
16. W. H. Sorrell, *Monthly Notices Royal Astron. Soc.* **334**, 705 (2002).
17. B. Freytag, F. Allard, H. G. Ludwig, et al., *Mem. della Soc. Astron. Italiana* **80**, 670 (2009).
18. B. Freytag, F. Allard, D. Homeier, et al., *ASP Conf. Ser.*, **450**, 125 (2011).
19. B. B. Ochsendorf, S. Verdolini, N. L. J. Cox, et al., *Astron. and Astrophys.* **566**, A75 (2014).
20. B. B. Ochsendorf, N. L. J. Cox, S. Krijt, et al., *Astron. and Astrophys.* **563**, A65 (2014).
21. N. Murray, E. Quataert, and T. A. Thompson, *Astrophys. J.* **709**, 191 (2010).
22. A. Ferrara, *Astrophys. J.* **407**, 157 (1993).
23. S. Bianchi and A. Ferrara, *Monthly Notices Royal Astron. Soc.* **358**, 379 (2005).
24. G. B. Field, *Astrophys. J.* **165**, 29 (1971).
25. M. R. Krumholz and T. A. Thompson, *Astrophys. J.* **760**, 155 (2012).
26. L. D. Anderson, A. Zavagno, L. Deharveng, et al., *Astron. and Astrophys.* **542**, A10 (2012).
27. V. S. Shevchenko, O. V. Ezhkova, M. A. Ibrahimov, et al., *Monthly Notices Royal Astron. Soc.* **310**, 210 (1999).
28. B. T. Draine and E. E. Salpeter, *Astrophys. J.* **231**, 77 (1979).
29. O. Plekan, A. Cassidy, R. Balog, et al., *Physical Chemistry Chemical Physics* **13**, 21035 (2011).
30. B. T. Draine, *Physics of the Interstellar and Inter-galactic Medium* (Princeton Univ. Press, Princeton, 2011).
31. E. Krügel, *The Physics of Interstellar Dust* (IOP Publishing, Bristol and Philadelphia, 2003).
32. H. C. van de Hulst, *Light Scattering by Small Particles* (Wiley & Sons, New York; Chapman & Hall, London; 1957).
33. A. Laor and B. T. Draine, *Astrophys. J.* **402**, 441 (1993).
34. B. P. Briegleb and B. Light, Technical note NCAR/TN-472+STR (National Center for Atmospheric Research, Boulder, CO, 2007).
35. D. Mihalas and B. W. Mihalas, *Foundation of Radiation Hydrodynamics* (Oxford Univ. Press, New York, 1984).
36. L. Pan and P. Padoan, *Astrophys. J.* **692**, 594 (2009).
37. P. A. R. Ade et al. (Planck Collab.), *Astron. and Astrophys.* **536**, A25 (2011).
38. B. T. Draine, in *The Cold Universe*, Ed. by A. W. Blain, F. Combes, B. T. Draine, et al. (Springer, 2004), Saas-Fee Advanced Course, Vol. 32, pp. 213–304.
39. C. F. Bohren and D. R. Huffman, *Absorption and Scattering of Light by Small Particles* (Wiley & Sons, New York, 1983).
40. B. Michel, Th. Henning, R. Stognienko, et al., *Astrophys. J.* **468**, 834 (1996).
41. <http://www.astro.princeton.edu/~draine/dust/dust.diel.html>
42. J. Dorschner, B. Begemann, T. H. Henning, et al., *Astron. and Astrophys.* **300**, 503 (1995).
43. R. Siegel and J. R. Howell, *Thermal Radiation and Heat Transfer* (McGraw Hill Book Company, New York, 1972).
44. J. H. Joseph and W. J. Wicombe. *J. Atmospheric Sci.* **33**, 2452, (1976).
45. W. J. Wicombe, *Delta-Eddington Approximation for a Vertically Inhomogeneous Atmosphere* (National Center for Atmospheric Research, 1977).
46. J.-L. Tassoul, *Theory of Rotating Stars* (Princeton Univ. Press, Princeton, 1978).
47. G. Zasowski, S. R. Majewski, R. Indebetouw, et al., *Astrophys. J.* **707**, 510 (2009).
48. G. A. Goncharov, *Astronomy Letters* **39**, 83 (2013).
49. G. A. Goncharov, *Astronomy Letters* **39**, 550 (2013).

*Translated by N. Oborina*